ADVANCED MATERIALS
www.advmat.de

Programming Cellular Alignment in Engineered Cardiac Tissue via Bioprinting Anisotropic Organ Building Blocks

*John H. Ahrens, Sebastien G. M. Uzel, Mark Skylar-Scott, Mariana M. Mata, Aric Lu, Katharina T. Kroll, and Jennifer A. Lewis**

The ability to replicate the 3D myocardial architecture found in human hearts is a grand challenge. Here, the fabrication of aligned cardiac tissues via bioprinting anisotropic organ building blocks (aOBBs) composed of human induced pluripotent stem cell derived cardiomyocytes (hiPSC-CMs) is reported. A bioink composed of contractile cardiac aOBBs is first generated and aligned cardiac tissue sheets with linear, spiral, and chevron features are printed. Next, aligned cardiac macrofilaments are printed, whose contractile force and conduction velocity increase over time and exceed the performance of spheroid-based cardiac tissues. Finally, the ability to spatially control the magnitude and direction of contractile force by printing cardiac sheets with different aOBB alignment is highlighted. This research opens new avenues to generating functional cardiac tissue with high cell density and complex cellular alignment.

1. Introduction

The human heart pumps blood through a circulatory network that distributes oxygen and nutrients throughout our body. Its contractile function arises from the myocardium. Within the left ventricular myocardium, individual cardiomyocytes contract uniaxially, but their complex transmural alignment gives rise to a torsional response that enhances global ventricular function.[1,2] In instances of heart disease or myocardial infarction, pathological remodeling can disrupt this cellular alignment and reduce contractile function.[3–6] The ability to mimic the cellular composition and complex alignment of human cardiac tissue is crucial for generating physiologically relevant tissues for drug discovery, disease modeling, and therapeutic repair.

To date, several methods have been developed to induce alignment in engineered cardiac tissues.[7–11] One common approach is to seed cardiomyocytes onto micro- or nanopatterned surfaces that contain topographical cues, which guide cellular alignment.[12,13] Another approach is to seed cells onto anisotropic polymer scaffolds[14–16] or decellularized matrices[17] that guide tissue alignment. In addition, cell-laden hydrogels seeded into molds of varying geometry can self-assemble into aligned cardiac rods, rings, bundles, and sheets.[18–24] Unfortunately, these methods are typically confined to thin cardiac tissues (≤100 µm thick) with either linear or radial alignment. By contrast, extrusion-based bioprinting offers broad flexibility to control tissue composition and architecture. Recently, we and others have demonstrated that synthetic and biological fibers exhibit shear-induced alignment during printing, opening the possibility to program tissue alignment via cell templating.[25–34] However, programming the architecture of human tissues by directly aligning anisotropic tissue building blocks has yet to be explored.

Here, we report the fabrication of engineered cardiac tissue with programmable alignment via bioprinting of anisotropic organ building blocks (aOBBs) (**Figure 1**). These aOBBs are elongated microtissues composed of cellular aligned hiPSC-CMs that can be modularly assembled into a printable bioink (Figure 1a). Individual aOBBs within this bioink align along the print path due to the same shear and extensional forces that orient acellular fibers upon extrusion through a tapered nozzle (Figure 1b).[35] Using this method, we fabricated cardiac tissues with high cellular density and programmed alignment across multiple length scales; ranging from individual aOBBs to the sarcomeric machinery that drives their contractile function (Figure 1c).

2. Results and Discussion

The first step in creating our cardiac bioink is to fabricate scalable micropillar arrays by stereolithography (SLA). These micropillar arrays are used to generate tens of thousands of aOBBs with controlled aspect ratio and cellular composition. After optimizing these parameters, we employed a sequential transfer micromolding process to create a single contiguous

J. H. Ahrens, S. G. M. Uzel, M. Skylar-Scott, M. M. Mata, A. Lu, K. T. Kroll, J. A. Lewis
John A. Paulson School of Engineering and Applied Sciences and Wyss Institute for Biologically Inspired Engineering
Harvard University
Cambridge, MA 02138, USA
E-mail: jalewis@seas.harvard.edu
J. H. Ahrens, S. G. M. Uzel, M. Skylar-Scott, M. M. Mata, A. Lu, K. T. Kroll, J. A. Lewis
Wyss Institute for Biologically Inspired Engineering
Harvard University
Cambridge, MA 02138, USA
The ORCID identification number(s) for the author(s) of this article can be found under https://doi.org/10.1002/adma.202200217.

DOI: 10.1002/adma.202200217

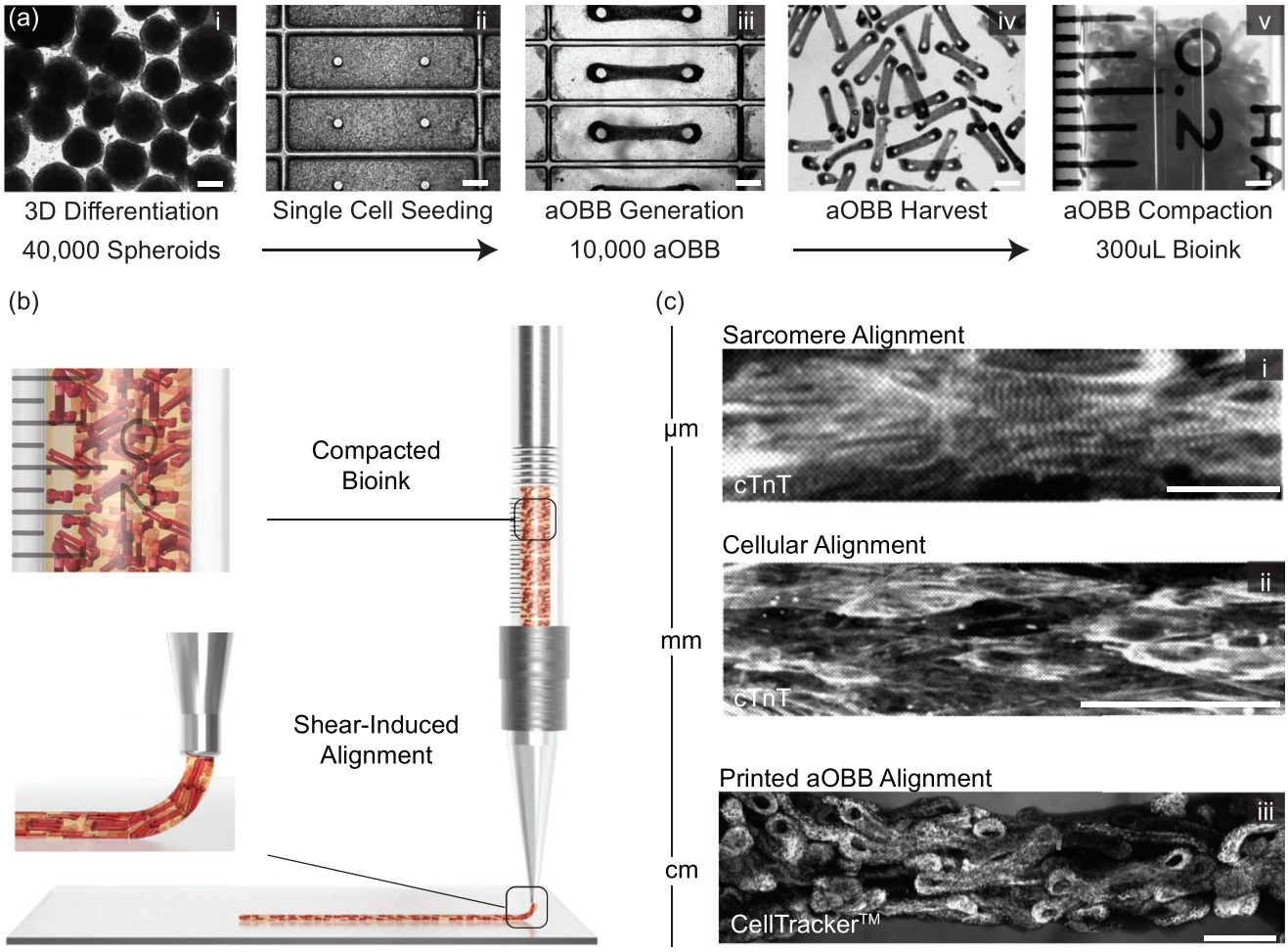

Figure 1. Aligned cardiac tissues via bioprinting. a) Image sequence highlighting the key steps in cardiac bioink preparation: Step: i) Human induced pluripotent stem cell (hiPSC) derived cardiac spheroids are generated and then dissociated into hiPSC derived cardiomyocytes (hiPSC-CMs); ii) hiPSC-CMs are combined with human neonatal dermal fibroblasts (hNDFs) in a 9:1 ratio, suspended in collagen-based gel, and seeded into micropillar arrays; iii) the cells self-assemble into aOBBs; and iv,v) aOBBs are then harvested and compacted in a syringe. Scale bars: i): 200 μm; ii,iii): 500 μm; and iii,iv): 1000 μm. b) Schematic illustration of aOBB orientation within the compacted bioink, which depicts their initial random orientation in the syringe reservoir followed by their shear-induced alignment during ink extrusion from nozzle. c) Multiscale alignment generated via bioprinting cardiac inks composed of aOBBs where: i) sarcomere alignment is observed within each cell; ii) individual cells are aligned within aOBBs; and iii) aOBBs are aligned within a bioprinted tissue. Scale bars: i) 20 μm; ii) 100 μm; and iii) 2 mm.

elastomeric plate with $n = 1050$ micropillar wells (Figure S1, Supporting Information). To our knowledge, this pillar platform provides the largest replicate value (n) reported to date. Next, we followed a previously reported protocol to generate embryoid bodies from hiPSCs, which are subsequently differentiated into cardiac spheroids and dissociated into cardiomyocytes (Figure S2, Supporting Information). we utilized this 3D differentiation protocol to scalably and efficiently obtain hiPSC-CMs. After dissociation, the hiPSC-CMs are combined with an appropriate number of hNDFs to achieve either a 0:1 (model) or 9:1 ratio. These cells are then resuspended in a collagen I solution at a concentration of 10^6 cells mL^{-1} and seeded into the micropillar arrays to generate densely cellular, cardiac microtissues that serve as aOBBs (Figure S3, Supporting Information). Within three days of seeding (9:1 iPSC-CM:hNDF ratio), the self-assembled aOBBs are synchronously contractile and their iPSC-CMs exhibit aligned sarcomeres, as visualized by immunofluorescent staining, and quantified via Fourier analysis (Figure S4, Supporting Information). After harvesting the aOBBs from the micropillar arrays, they are resuspended in a mixture of processed gelatin and fibrinogen in which gelatin serves as a rheological modifier during printing, while fibrinogen provides structural support after polymerization. Finally, the aOBB-laden suspension is compacted to create a densely cellular bioink.

To demonstrate our ability to direct aOBB alignment, we bioprinted tissues in both cylindrical and sheet-like geometries from bioinks composed of either fibroblast (0:1 iPSC-CM:hNDF ratio) or cardiac (9:1 iPSC-CM:hNDF ratio) aOBBs. we prelabelled these aOBBs with fluorescent cell trackers and used confocal microscopy to visualize their alignment within the dense cylindrical tissues (**Figure 2**). we quantified their alignment by overlaying each aOBB with a volumetric 3D model and extracting their primary orientation relative to the print

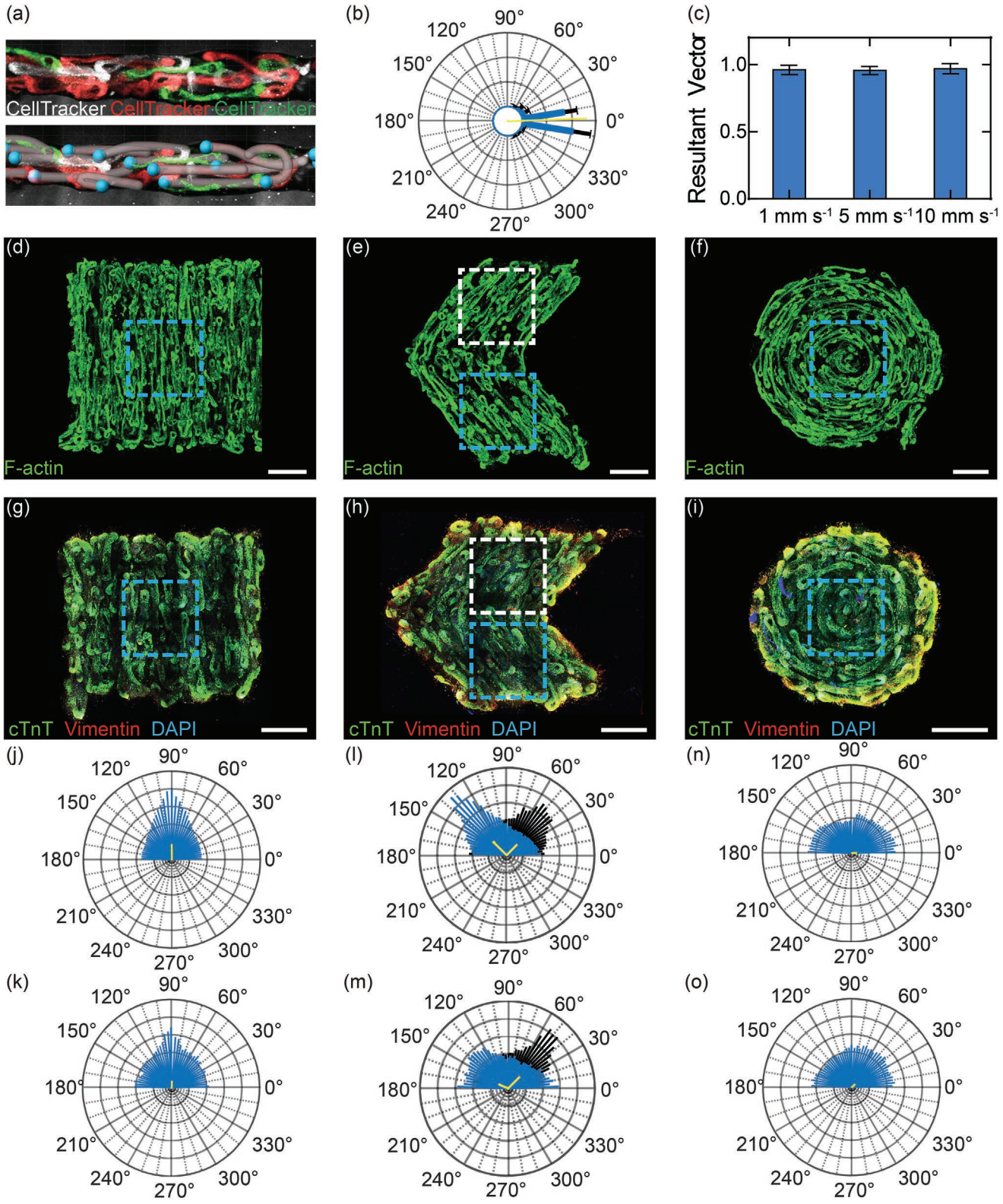

Figure 2. Programming complex alignment in model and cardiac tissues. a) Visualization of pre-labelled anisotropic organ building blocks (aOBBs) printed at 5 mm s^{-1} and 3D volumetric models. b) Polar histogram of aOBB orientations. The yellow bar indicates the resultant vector. c) Quantification of the spread of aOBB orientation as a function of print speed (1–10 mm s^{-1}). d–f) 3D bioprinted, hNDF-based model sheets with varying patterns. Scale bars: 2000 µm. g–i) 3D bioprinted, cardiac-based sheets with varying patterns. Scale bars: 2000 µm. Polar histograms for aOBB orientation in vertical (j,k), chevron (l,m), and circular (n,o) patterned sheets. The top row (j,l,n) and bottom row (k,m,o) correspond to hNDF and cardiac sheets, respectively. All the yellow bars indicate resultant vector lengths.

direction (Figure 2a). For fibroblast-based cylindrical tissues bioprinted at 5 mm s^{-1}, we find that the mean orientation angle of these aOBBs plotted in a polar histogram is centered ≈0°, which corresponds to the printing direction (Figure 2b). Importantly, we observed a high degree of aOBB alignment across a broad range of print speeds (1–10 mm s^{-1}) (Figure 2c), indicating that these soft, densely cellular aOBBs are capable of shear-induced alignment during bioprinting. Harnessing this capability, we created both fibroblast (Figure 2d–f) and cardiac (Figure 2g–i) tissue sheets composed of linear, chevron, and spiral patterned architectures with programmed aOBB alignment. Fourier analysis is applied to confocal images of immunofluorescently stained tissue sheets to determine the primary orientation of aOBBs. Using polar histograms, we characterized their axial distribution, mean orientation angles, and resultant vector lengths. The vertical patterned tissue sheets exhibited a mean orientation angle near 90° (Figure 2j,k), while the chevron patterned tissue sheets exhibited two primary orientation angles near 45°/135° (Figure 2l,m). Moreover, the distribution of aOBB orientations for the vertical and chevron patterned sheets demonstrated narrow peaks with correspondingly high resultant vector lengths, visualized as the length of the yellow bars overlaying the polar histograms. By contrast, the circular patterned sheets exhibited a much broader and more uniform distribution of orientation angles, as indicated by the associated low resultant vector lengths (Figure 2n,o).

To facilitate long-term culture and functional characterization, we printed cardiac macrofilaments composed of aOBBs onto custom-designed, elastomeric macropillar platforms (Movie S1, Supporting Information). In addition, we bioprinted spheroidal OBBs that are assembled in pillarless arrays seeded with the same cellular and extracellular matrix composition as their anisotropic counterparts. Upon compaction, the spheroids demonstrated isotropic cellular alignment and served as a control for downstream functional assays. The platforms are designed such that bioprinted cardiac macrofilaments are stably positioned at the top of elastomeric pillars, which enabled the measurement of pillar deflection and, hence, contractile force over time (Figures S5 and S6, Supporting Information). After platform assembly, a sacrificial gelatin layer is first added to support the macrofilament during bioprinting. After bioprinting is completed, fibrinogen present within cardiac macrofilaments is subsequently polymerized by adding 4 °C, thrombin-rich media followed by incubation at 37 °C. As the temperature increases, the gelatin within the extracellular matrix (ECM) of the bioprinted cardiac tissue melts, facilitating thrombin diffusion and fibrin polymerization. During polymerization, the sacrificial gelatin layer also melts and is subsequently removed, resulting in an aligned, densely cellular (>200 × 10^6 cells mL^{-1}), contractile cardiac macrofilament suspended between silicone pillars (**Figure 3**a, and Figure S7, Supporting Information).

Immediately after bioprinting, cardiac macrofilaments composed of aOBBs exhibited a preferred cellular alignment along the printing direction that was roughly threefold higher than the spheroid-based controls (Figure 3b–d). we attribute this preferential alignment to the shear-induced orientation of aOBBs. However, after 7 days in culture, we observed dramatic cellular reorientation in both types of bioprinted cardiac macrofilaments (Figure 3e). This analysis was conducted using confocal images of whole mount, stained cardiac macrofilaments that largely depict the cells on the surface or periphery. However, cryo-sectioned slices, which are representative of the tissue mid-plane, revealed far less cellular reorientation (Figure 3f,g, and Figure S8, Supporting Information). we hypothesize that cells on the periphery of these cardiac macrofilaments can reorient parallel to passive stress lines that arise due to cellular compaction, while reorientation in the tissue core is hindered by surrounding cells and extracellular matrix.[36,37]

Next, we characterized the fusion of anisotropic and spheroidal OBBs into electromechanically synchronous cardiac tissue. Fluorescent-based calcium imaging is used to visualize action potential propagation throughout bioprinted cardiac macrofilaments (Movies S2 and S3, Supporting Information). Day 1 after printing, the contractile wave of all cardiac macrofilaments exhibited a smooth propagation front (**Figure 4**a). While the observed propagation in all macrofilaments demonstrated a distinct directionality, the conduction velocity (CV) was very slow (≈5 mm s^{-1}). Since the bioprinted macrofilaments are 1 cm in length, the slow CV resulted in asynchronous contraction of the discrete anisotropic and spheroidal OBBs. The incomplete recruitment of OBBs during each contractile cycle is represented by a wide range of recorded pillar displacement values on Day 1 (Figure S9, Supporting Information). As the macrofilaments remodeled, we observed fully synchronous contraction by Day 3 along with more uniform macropillar displacement values. As revealed by isochrone activation maps on Day 4 after printing, the CV increased dramatically in both the anisotropic and spheroid-based cardiac macrofilaments (Figure 4b,c). On Day 4, we also observed Connexin-43 positive gap junctions (Figure S10a, Supporting Information) and N-Cadherin positive adherens junctions (Figure S10b, Supporting Information) between cardiomyocytes, which is indicative of tissue fusion. Protein expression also reveals the upregulation of multiple cardiac specific genes, including Connexin-43 by Day 4 (Figure S11, Supporting Information).

By applying Euler–Bernoulli beam theory, we extracted contractile force values from the macropillar deflections (Figure S12 and Movies S4 and S5, Supporting Information). Importantly, we find that cardiac macrofilaments composed of aOBBs generate a higher contractile force compared to spheroid-based controls (Figure 4d). To further highlight the functional effect of directing cellular alignment, we sought to normalize the macrofilament force per cardiomyocyte. As anisotropic particles are unable to compact as densely compared to spheroids,[38] we quantified the number of cardiomyocytes within each type of microfilament by flow cytometry (Figure S13, Supporting Information). Immediately after printing, aOBB-based macrofilaments contain roughly 50% fewer cardiomyocytes compared to spheroid-based controls. Since iPSC-CMs are known to have low proliferation rates,[39] we normalized the measured force across all time points by the number of cardiomyocytes within each type of bioprinted tissue on Day 0. Based on this normalization, we find that the aligned cardiomyocytes within the aOBB-based macrofilaments exhibit a threefold higher contractile force compared to the less aligned cardiomyocytes in spheroid-based controls (Figure 4e). we also normalized force by measuring tissue stress. On Day 7 after bioprinting, we observed a twofold higher stress value in the aligned cardiac macrofilaments

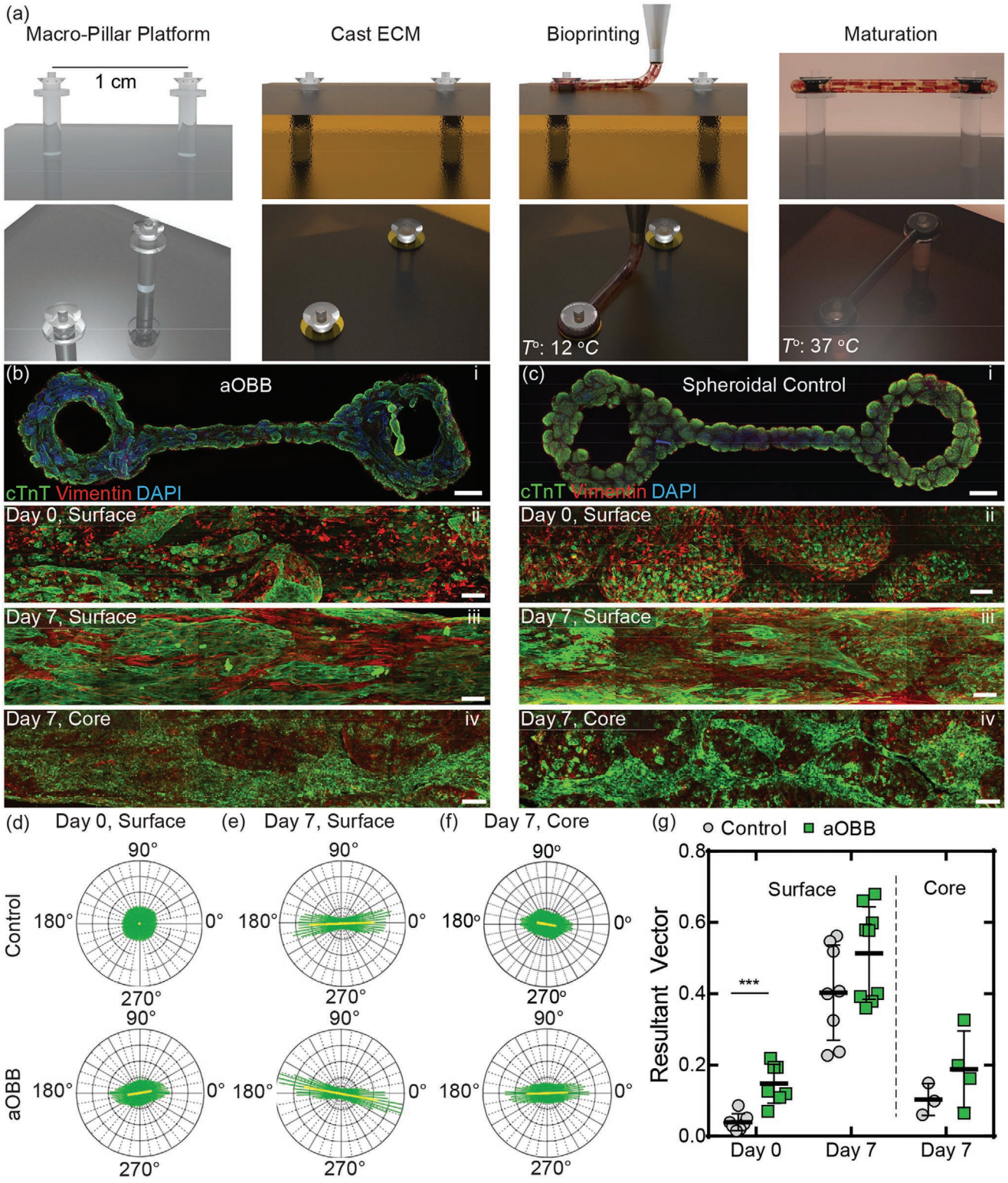

Figure 3. Aligned cardiac macrofilaments. a) Schematic overview of the bioprinting process used to generate aligned cardiac macrofilaments on macro-pillars. b,c) Visualization of cellular alignment within bioprinted cardiac macrofilaments composed of aOBBs (b) and control spheroids (c). i) Day 0, 5×; ii) tissue surface, Day 0, 20×; iii) tissue surface, Day 7, 20×; and iv) tissue core, Day 7, 20×. Scale bars: i) 1000 µm; and ii–iv) 100 µm. d–f) Polar histograms display primary orientations extracted from high-magnification (20×) images of anisotropic and spheroid-based cardiac macrofilaments. The yellow bars represent resultant vectors. g) Resultant vectors indicate distribution of polar histogram data from 20× images; *p*-values are calculated using multiple *t*-tests with a Holm–Sidak correction, ***$p < 0.001$.

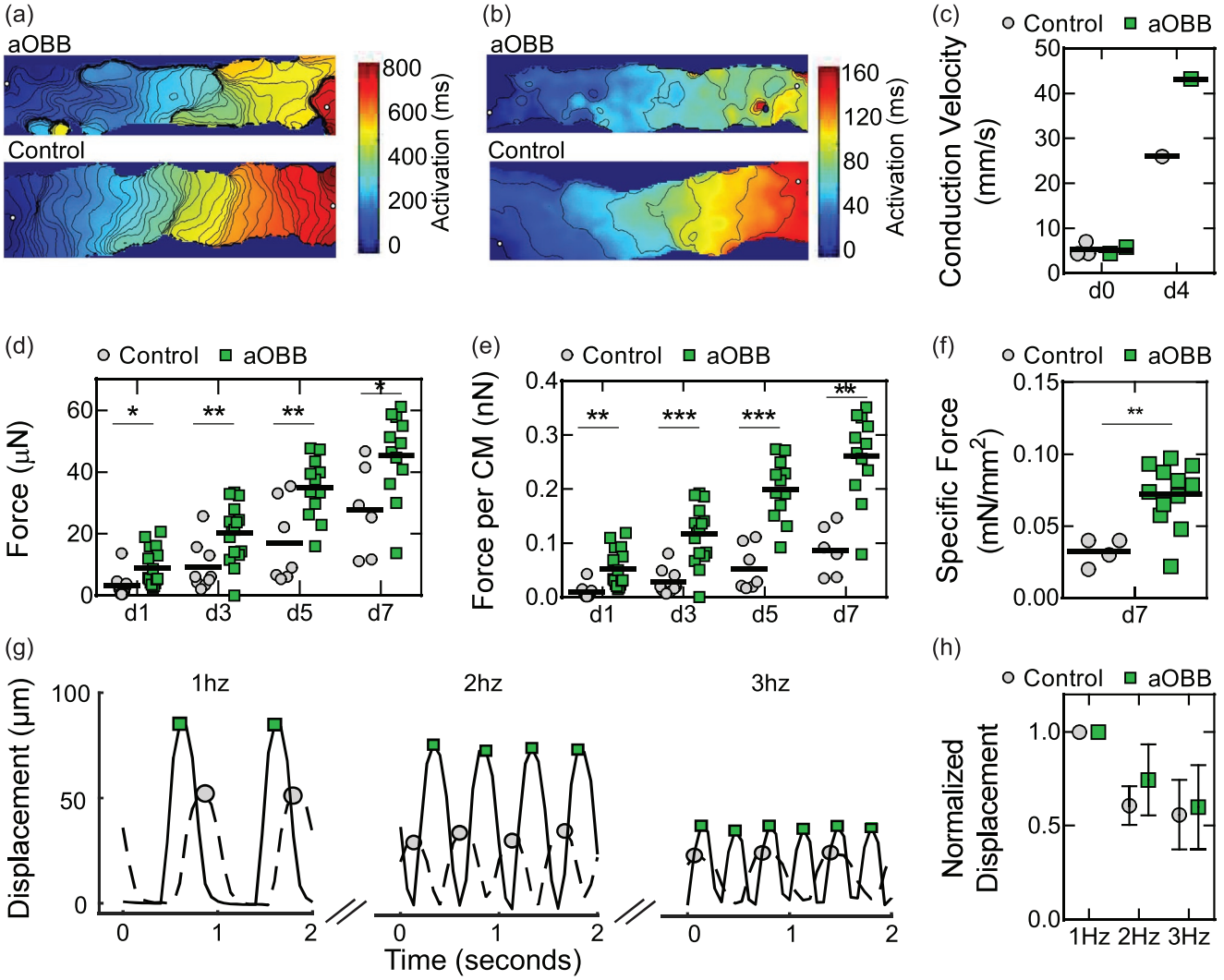

Figure 4. Functional characterization of aligned cardiac macrofilaments. Activation maps derived from calcium imaging of bioprinted cardiac macrofilaments composed of aniostropic and spheroidal OBBs at Day 0 (a) and Day 4 (b). c) Conduction velocity measurements derived from activation maps. d) Force measurements of bioprinted tissues over time; bar presented as mean, *p*-values are calculated using multiple *t*-tests with Holm–Sidak correction, $*p < 0.05$, $**p < 0.01$. e) Force normalized per input cardiomyocyte; *p*-values are calculated using multiple *t*-tests with Holm–Sidak correction, $**p < 0.01$, $***p < 0.001$. f) Force on Day 7 normalized by cross-sectional area; *p*-value is calculated using *t*-test, $**p < 0.01$. g) Representative displacement graphs of electrically stimulated bioprinted tissues (1–3 Hz). h) Force–frequency relationship for electrically stimulated, bioprinted tissues; data are presented as mean ± SD, $n = 5$ for control, $n = 6$ for aOBB.

composed of aOBBs compared to spheroid-based controls (Figure 4f). To further assess their functional capacity, we used electrical field stimulation to pace these aligned cardiac macrofilaments at frequencies up to 3 Hz (Movie S5, Supporting Information). While both types of cardiac macrofilaments maintain electrical pacing at 1–2 Hz, only aligned cardiac macrofilaments composed of aOBBs can maintain electrical pacing at 3 Hz (Figure 4g, and Movie S6, Supporting Information). In both cases, a negative force–frequency relationship is observed (Figure 4h), which is consistent with observations from other stem-cell-derived cardiac tissues at similar time points.[40]

As a final demonstration, we printed cardiac tissue sheets composed of aOBBs aligned either 0° (parallel) or 90° (perpendicular) to silicone macropillars (**Figure 5**a,b, and Movies S7 and S8, Supporting Information). After Day 1 in culture, cardiac tissue sheets with parallel aOBB alignment exerted more than twice the contractile force compared to those printed with perpendicular aOBB alignment (Figure 5c). While some re-orientation occurs over time, cardiac tissue sheets with parallel aOBB alignment continue to exert a higher average contractile force over a two-week period reflecting the persistence of their programmed alignment. Finally, we demonstrated that the contractile frequency of these cardiac tissue sheets increases upon incubation in isoproterenol, a known β-adrenergic agonist (Figure 5d,e).

3. Conclusion

We report a scalable biofabrication method to generate stem-cell-derived, engineered cardiac tissue with high cellular

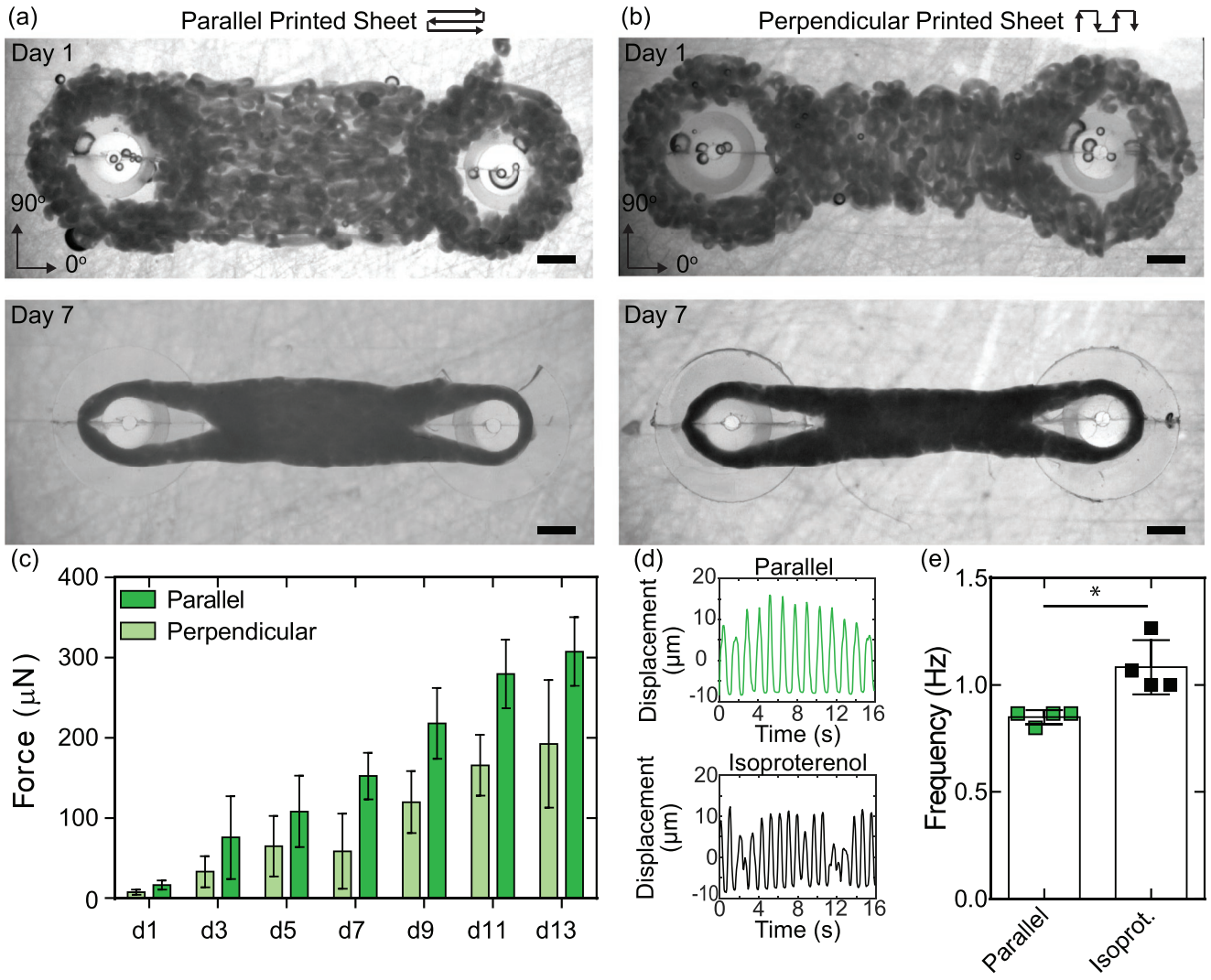

Figure 5. Longitudinal culture and functional characterization of aligned cardiac sheets. Bioprinted cardiac tissue sheets composed of aOBBs aligned parallel (0°) (a) and perpendicular (90°) (b) to macropillar anchors. Scale bars: 1 mm. c) Force generation as measured by macropillar deflection; data are presented as mean ± SD, $n = 4$. d) ß-adrenergic stimulation via isoproterenol incubation increases their contractile frequency; data are presented as mean ± SD, p-value calculated using t-test, $^{*}p < 0.05$. e) Spontaneous contraction pattern for aligned cardiac tissues before (top) and after administering 10×10^{-6} M isoproterenol.

density and programmed alignment. we created bioinks composed of large quantities of aOBBs that were pre-assembled on micropillar arrays. Next, we demonstrated that these aOBBs could be programmably aligned along the print direction by constructing both cardiac macrofilaments and sheets. Importantly, their programmed cellular alignment resulted in enhanced contractile function compared to spheroid-based cardiac tissues. Finally, we highlighted the ability to spatially control the magnitude and direction of contractile force in printed cardiac tissue sheets with different aOBB orientation. This advance represents an important step towards our ultimate goal of fabricating aligned, vascularized cardiac tissues for therapeutic use.

4. Experimental Section

Cells, Embryoid Bodies, and Spheroids: We obtained BJFF hiPS cell line from Jain at Washington University. They maintained this cell line and used these cells to create hiPSC-CMs following the protocols described in prior work.[41] Briefly, hiPSCs were cultured daily in supplemented mTeSR media (STEMCELL Technologies) at 37 °C/5.5% CO_2. hiPSCs were passaged every 4 days (when 80% confluency was reached) or used for embryoid body (EB) formation and cardiomyocyte differentiation. On passage days, the cells were rinsed in PBS without Ca^{2+} or Mg^{2+} (PBS−/−) and then rinsed with enzyme-free dissociation reagent ReleSR (STEMCELL Technologies). After immediate aspiration of ReleSR, hiPSCs were incubated at 37 °C/5.5% CO_2 for 8 min. Following this short incubation, the cells were gently resuspended in mTeSR media to dislodge hiPSCs as cell clusters and transferred to T225 culture flasks freshly coated with Matrigel (Corning) at a split ratio of 1:8. They also cultured hNDFs (Cascade Biologics) in Dulbecco's modified Eagle medium (DMEM, Gibco) supplemented with 1% penicillin–streptomycin and 10% fetal bovine serum (Gibco) at 37 °C/5.5% CO_2. Culture media was replaced every 2 days. For passage days, hNDFs were rinsed in PBS (−/−), then incubated for 5 min with TrypLE cell disassociation reagent (ThermoFisher Scientific). Cells were then washed in supplemented DMEM and split at 1:10 culture ratio in T225 culture flasks (Falcon) once weekly (at 80% confluency) or were otherwise used for experiments.

Cell viability prior to each experiment was quantified by AO/PI using an automated cell counter (Auto2000, Nexcelom).

Next, we generated embryoid bodies (EBs) following our prior protocol. Briefly, on Day 2 of differentiation, hiPSCs were transferred into AggreWell arrays to induce aggregation. The AggreWell arrays were first rinsed in isopropanol followed by autoclave-sterilization. Next, 2 mL of 0.2% Pluronic (Sigma) was added, followed by two rinses with DMEM/F12 (+HEPES and L-glutamine, GIBCO). 1 mL of PVA medium (mTeSR + 4 mg mL^{-1} polyvinyl alcohol) and 10×10^{-6} M of rho-associated coiled-coil forming kinase inhibitor (Y-27635, Biogems) was then added to each well. To prepare hiPSCs, the cells were rinsed with PBS (−/−) followed by a 12 min incubation with Gentle Cell dissociation reagent (STEMCELL Technologies) to dislodge growing culture colonies from T225 culture flasks. The cells were then resuspended in DMEM/F12 medium, transferred into a 50 mL conical tube, and centrifuged at 240 *g* for 5 min. The hiPSC pellet was resuspended in 12 mL PVA medium $+10 \times 10^{-6}$ M Y-27635. hiPSCs were evenly distributed into 2 AggreWell arrays per each T225 culture flask. Finally, AggreWell plates with hiPSCs were centrifuged at 100 *g* for 3 min and then placed in the incubator to aggregate at 37 °C/5.5% CO_2.

Finally, we used these hiPSC EBs to generate cardiac spheroids following a protocol that modulates Wnt/β-Catenin pathways (Figure S2, Supporting Information).[42] Briefly, on Day 0 of differentiation, hiPSC media was removed from each T25 flask by rinsing and resuspending the EBs in 5×10^{-6} M of WNT activator CHIR (CHIR 99 021, Biogems) diluted in cardiac differentiation media (CDM) that consisted of basal RPMI-1640 (Gibco) supplemented with 2% B27/-insulin supplement (ThermoFischer Scientific). Fresh supplemented CDM media was added on Day 1. CHIR was removed on Day 2 by rinsing and resuspending the spheroids in CDM only. On Days 3 and 4, spheroids were cultured with 2×10^{-6} M of WNT inhibitor iWR1(Biogems) in CDM. On Day 5 iWR1 was removed by rinsing and the spheroids were cultured in CDM only through Day 6. From Day 7 to Day 9, the spheroids were cultured in cardiac maturation medium (CMM, 2% B27 [ThermoFisher Scientific] in RPMI-1640). Lastly, from Day 9 to 11, to metabolically purify the hiPSC-CMs, spheroids were cultured in RPMI without glucose (Gibco) supplemented with 2% B27 and 4×10^{-3} M lactate (Sigma). All steps highlighted from Day 0 to Day 11 were performed with spheroids cultured in T25 flaks in an orbital shaker at 53 revolutions per minute (rpm) and at 37 °C/5.5% CO_2.

Micropillar Array Fabrication: Micropillar arrays are used to generate cardiac or fibroblast aOBBs. To generate a scalable number of aOBBs (≈10 000 per experiment), we created polydimethylsiloxane (PDMS, Sylgard 184, Dow Corning) plates that contained 1050 micropillar arrays. Plates were designed to fit inside Nunc OmniTray-well plates that are compatible with conventional imaging equipment. The first step in this fabrication process was to print a single rectangular mold that contained 175 micropillar arrays using a stereolithographic (SLA) 3D printer (Perfactory Aureues Plus, EnvisionTec) using their photo-curable resin HTM140 V2. To increase their mechanical strength, the SLA-printed rectangular molds were UV post-cured for 5 min (OmniCure, Excelitas). Prior to the UV exposure, the molds were heated on a hot-plate to 80 °C, beyond the glass-transition temperature (T_g) of the cured resin. Next, the mold surface was covalently modified with fluorosilane (1H,1H,2H,2H-perfluorooctyltriethoxysilane 97%, Oakwood Chemical) to ensure proper PDMS curing during the transfer molding process. Briefly, to prepare the device for salinization, it was first plasma treated with the following settings: 5 min plasma, 100% O_2, 100% power (Femto, Diener). After plasma treatment, the rectangular mold was immediately transferred to a vacuum chamber containing fluorosilane, where it remained under vacuum for a minimum of 2 h. The next step in the fabrication process was to generate reusable elastomeric negatives of these micropillar array molds. First, the six SLA-printed molds were placed in laser-cut acrylic holders designed to fit snugly into a Nunc 1-well plate (ThermoFischer Scientific). To generate a negative mold, a flexible and strong silicone (SortaClear37, Smooth-On) was formulated at 1:1 (PartA:PartB) mass ratio with 2% (Part A + Part B) SloJo (SmoothOn) to increase pot-life and 10% (Part A) SilioneThinner (SmoothOn) to reduce viscosity. These components were mixed via centrifugation in a SpeedMixer (FlackTek Inc.) for 3 min at 2000 *g*. The silicone was then poured over the six (contiguous) SLA-printed molds and acrylic holder. The plate was then degassed in a vacuum chamber for 1 min and left overnight at room temperature to cure. The negative micropillar array plate was removed manually from the mold. To enable the subsequent silicone-on-silicone transfer molding process, the same fluorosilane surface modification was repeated for the negative micropillar array plate. In addition, after the plate was taken out of the vacuum, it was post-cured at 80 °C for 2 h. After the post-curing process, the negative plate was placed back into the Nunc 1-well plate. Finally, PDMS mixed at 10:1 (base:catalyst) mass ratio was poured into this negative mold, degassed for 5 min in a vacuum, and then polymerized for 3 h at 80 °C. The final PDMS micropillar array plate was removed manually and autoclaved prior to use.

Anisotropic OBB Generation: To generate aOBBs, we first prepared the PDMS micropillar array plates for cell seeding. Each PDMS plate was plasma treated for 1 min in 100% O_2 gas at full power (Femto, Diener) to increase hydrophilicity and wetting. Immediately after plasma treatment, anti-adhesion rinsing solution (STEMCELL Technologies) is added to each well, where it remained for >30 min at room temperature. After 30 min, they aspirated the rinsing solution and washed the plates twice with DMEM/F12 (+HEPES and L-glutamine, GIBCO).

After preparation of the PDMS micropillar array plates, we dissociated the cardiac spheroids into single cells. It is critical to dissociate cardiac spheroids using as soft an enzymatic solution as possible to increase viability of iPSC-CMs. In addition, all serological pipette tips should be treated with 3% bovine serum albumin (BSA, Sigma) to prevent adhesion and loss of cardiac spheroids. The first step in cardiac spheroid dissociation is to incubate spheroids in 1 mg mL^{-1} solution of CollagenaseB (Sigma) diluted in Earle's Balanced Salt Solution (EBSS, ThermoFischer). 10 mL of 1 mg mL^{-1} CollagenaseB solution is made per an estimated 20×10^6 cells. The calcium concentration of CollagenaseB is adjusted to 5×10^{-3} M for enhanced enzymatic activity. First, cardiac spheroids are aggregated via gravity. The supernatant is aspirated and the cardiac spheroids are resuspended in CollagenaseB solution. The suspension is transferred to ultralow attachment 6 well plates (Corning) and incubated for 1 h at 37 °C/5.5% CO_2, on an orbital shaker set to 53 rpm. After 1 h of incubation, the spheroids are aggregated in 50 mL tubes and diluted 1:1 in PBS without Ca^{2+} and Mg^{2+} (PBS −/−), to inactivate the calcium-dependent CollagenaseB. In addition, calcium is a co-factor for cell–cell binding and its sequestration enhances single cell dissociation. Each 50 mL tube is centrifuged at 240 *g* for 5 min and then washed in 50mL PBS −/−.

The second step in dissociation is to enzymatically digest the cardiac spheroids using TrypLE Express (ThermoFischer). TrypLE Express solution is supplemented with 40 U mL^{-1} DNAseI (Worthington, Inc.). Cardiac spheroids are aggregated and incubated in 1 mL TrypLE Expression solution at 37 °C for 15 min. Prior to enzymatic inactivation, the spheroids are mechanically dissociated by pipetting ≈20× with P1000 pipette. After mechanical dissociation, the enzymatic solution is inactivated by diluting the sample in DMEM/F12. After centrifuging at 240 *g* for 5 min, the supernatant is aspirated, and the pellet resuspended in DMEM/F12. To ensure accurate cell counting, cellular aggregates are filtered by pipetting the resuspension through a 70 µm filter. Viability and cellular density are quantified using Cellometer Auto 2000 Automated Cell Counter (Nexcelom). The single cell suspension is kept on ice. Next, a monolayer of hNDFs are enzymatically dissociated into single cells and counted. Briefly, the monolayer is washed in PBS without Ca^{2+} and Mg^{2+} (PBS −/−). These cells are incubated in TrypLE solution for 10 min at 37 °C. After mechanical dissociation, the enzymatic solution is diluted in DMEM/F12 and centrifuged at 240 *g* for 5 min. After aspiration of the supernatant, the pellet is resuspended in DMEM/F12, and counted using a Cellometer Auto 2000 Automated Cell Counter. The single cell suspensions of iPSC-CMs and hDNFs are then combined in a 9:1 ratio iPSC-CMs:hNDFs. The corresponding volumes of each suspension are mixed and centrifuged at 240 *g* for 5 min and kept on ice.

Based upon the total concentration of iPSC-CMs, an appropriate volume of 1× rat tail collagen I (Corning) solution was prepared on ice.

An appropriate volume of collagen I was calculated based upon a desired final concentration of 1.25 mg mL^{-1}. Then *y*/100 mL of 250×10^{-3} M $CaCl_2$, ≈*x*/40 mL of 1 N NaOH, and *y* mL of collagen I were added, in order, to the basal DMEM high glucose media. After aspiration of the supernatant, the cellular pellet was resuspended in a volume of collagen gel that yielded a final concentration of 10^6 cell mL^{-1}. Next, 250 µL of the cell–gel suspension was pipetted into the middle of each PDMS well that contained 175 micropillar arrays. A sterilized microscope slide was then used to evenly distribute the cell–gel solution throughout the micropillar array. Due to the prior plasma treatment of the PDMS plate, the cell–gel solution wicked into the micropillar arrays easily (Figure S3, Supporting Information). After repeating this process for all micropillar arrays, the PDMS plate was incubated at 37 °C/5.5% CO_2 for 25 min. Finally, each well was filled with supplemented DMEM high glucose media and a final concentration of 10×10^{-3} M Y-27635.

Bioinks: We began by preparing ECM and media solutions. First, a 15% (*w*/*v*) gelatin stock solution (solubilized at 90 °C for 12.5h) was diluted to 5% gelatin (*w*/*v*) and combined with 15% fibrinogen (*w*/*v*). Second, 1 mL of 10% gelbrin (*w*/*v*) solution was prepared in DMEM/F12 (Gibco). Third, DMEM High Glucose + 10% FBS was supplemented with 50×10^{-6} M Y-27635 (Biogems). Fourth, 100 U mL^{-1} thrombin solution was prepared in DMEM High Glucose + 10% FBS. All ECM and media solutions were held at 37 °C using a hotplate. To chemically inhibit active compaction of the anisotropic OBBs and maintain their elongated structure, all aOBBs were incubated in the 50×10^{-6} M solution of Y-27653 for 1 h at 37 °C/5.5% CO_2. After 1 h, the aOBBs were harvested manually using a P1000 pipette with wide-bore tips. The wide-bore tips were treated with 3% BSA to prevent adsorption of the aOBBs. aOBBs were collected three wells at a time and transferred into a single 50 mL tube. Upon collection, the aOBBs were allowed to settle under gravity for 5 min. After the supernatant was aspirated, they estimate the volume (*g* mL) of compacted aOBBs. They subsequently wash compacted aOBBs in *3x* volume of gelbrin bioink. After mixing with the wide-bore pipette, the 50 mL tube was centrifuged in 50 mL at 100 *g* for 3 min. Next, the gelbrin supernatant was aspirated and resuspended in another 1× volume of the gelbrin solution.

The aOBB laden bioink was transferred into a modified 1.0-cm^3 glass syringe (Hamilton), which was pre-filled with ≈350 µL of the warmed 10% gelatin (*w*/*v*) and placed on ice for 1 min. Under ambient conditions, we loaded the bioink into the glass syringe through the drilled-out top followed by centrifugation for 1 min at 100 *g*. While the aOBBs were centrifuging, they attached a 1.5″ metal nozzle (Nordson EFD) to the aspirating line. After centrifugation, they aspirated the supernatant and added the remaining aOBB-laden bioink. They repeated this process until the bioink was fully loaded into the 1.0-cm^3 glass syringe. The ink was then centrifuged for 5 min at 200 *g* and the residual supernatant was removed. The gelatin-fibrinogen ECM within the compacted aOBB-laden bioink was physically crosslinked by cooling in a 4 °C fridge for 15 min.

Bioprinting of Aligned Cardiac Tissues: A custom-designed two-part mold for a 3D printing platform was designed and fabricated, which facilitated the 3D printing process and enabled long-term culture of tissue. The two-part mold was printed using a stereolithography 3D printer (Perfactory Aureus, Envisiontec. Inc.). The same photocurable resin (HTM140 V2, EnvisionTec) was used as was for the micropillar array fabrication. Design considerations included: 1) pillar caps and pillar ledges that maintained a consistent and reproducible z-height for the 3D printed filament; 2) internal shelfs in line with stability ledges for the addition of sacrificial gelatin substrate; 3) reference caps that served as a zeroing location for the nozzle to initiate 3D printing; and 4) complementary pins and holes designed for a slip fit connection of the two-part molds. To prevent inhibition of platinum-based curing of silicones, the SLA-printed molds were plasma treated and silanized (see above, Micropillar Array Fabrication). To form a single mold, the two SLA-printed parts were tightly sealed by inserting an M4 nut through the side compression channels and tightening using wing-nuts. Upon assembly, soft silicone was poured into the mold (EcoFlex-050, SmoothOn) at a 1:1 mass ratio PartA:PartB. The silicone was polymerized at room temperature for >3 h. The platform was de-molded by hand by unscrewing the M4 threads and disassembling the two-part mold. This device was autoclaved prior to use.

All bioinks were dispensed using a custom-built syringe pump, which was controlled via an Arduino microcontroller and a stepper-motor driver. The syringe barrel was housed in a water-cooled, custom-built temperature controller. Before printing, the syringe was incubated in the temperature-controlled housing for >15 min. Immediately prior to printing, a pre-chilled, tapered plastic nozzle with an inner diameter of 0.61 mm (Nordson EFD) was fitted to the bottom of the syringe. The bioink was held at ≈12 °C, where it exhibited optimal printing behavior. The extrusion rate of the syringe pump was set to define a filament diameter below 1 mm at a print speed of 5 mm s^{-1}. After printing, the tissues were incubated in a 4 °C fridge for 5 min to ensure that the ECM within the bioink solidified. Next, cold DMEM high glucose supplemented with 10% FBS and 20 U mL^{-1} thrombin was added to the tissue and the entire printing platform was incubated at 37 °C/5.5% CO_2. As the media increased in temperature, the thermally reversible gelatin in the bioink melted, which enabled the thrombin to simultaneously diffuse in and polymerize the fibrinogen into fibrin. After 1 h, the melted gelatin substrate was aspirated. Fresh DMEM high glucose + 10% FBS was added and the tissue was returned to 37 °C/5.5% CO_2.

Cell Viability Assays: Bioprinted cardiac macrofilaments were sectioned and transferred via pipette into a 35 mm Petri dish. The sectioned tissue was washed twice in standard PBS. Next, the tissue was incubated with Live/DEAD (ThermoFischer) solution (calcein-AM (2×10^{-6} M), ethidium-homodimer-1 (4×10^{-6} M)) and incubated at 37 °C/5.5% CO_2 for 30 min. After incubation, Live/DEAD images were acquired on a confocal microscope (ZEISS). (Figure S14, Supporting Information).

Immunostaining and Flow Cytometry: To prepare cardiac tissue for immunostaining, they were rinsed twice with standard PBS and fixed in a 4% paraformaldehyde (PFA) solution for 45 min at room temperature. After fixation, they were washed three times with PBS and blocked for 3 h in blocking solution (PBS, +5% (*w*/*v*) goat serum (GS), +0.25% (*w*/*v*) Triton-X). Following this incubation, the blocking solution was removed and aOBBs were rinsed twice with standard PBS. Next, the aOBBs were incubated for 48 h at 4 °C in TNNT2/cTnT primary antibody (ab45932, Abcam) at 1:400 dilution in staining solution (PBS, +1%GS, +0.25% Triton-X). The aOBBs were then washed three times with PBST (0.1% Tween-20 in PBS) and left overnight at 4 °C. The following day they were incubated with AlexaFluor-555 conjugated secondary antibody for 2 h. In the last 30 min of this incubation, Actin Green fluorescent probe (Invitrogen) was added according to manufacturer's instructions and 4′,6-diamidino-2-phenylindole (DAPI) nuclear stain was added at 1:3000 dilution. aOBBs were rinsed twice with PBST and remained in PBST at 4 °C before imaging.

Cardiac spheroids were prepared for flow cytometry analysis by first dissociating them into single cells, as described in a prior work.[41] Briefly, the spheroids were harvested on Day 11, washed in PBS, and incubated with CollagenaseB (1 mg mL^{-1}) for 1 h at 37 °C/5.5% CO_2. Next, they were rinsed twice in cold DMEM/F12 and incubated with 25 U mL^{-1} of papain (Worthington, Inc.) in Earle's Balanced Salt Solution (EBSS, +EDTA and L-cystein, Gibco) for 30 min at 37 °C/5.5% CO_2. Papain was inhibited with DMEM/F12 + 10% FBS. Next, cells were rinsed with DMEM/F12 and pipetted several times with a P1000 pipette. The dissociated cells were rinsed twice in standard PBS. 1×10^6 cells per condition were then incubated with fixable viability dye LIVE/DEAD Aqua (Thermofisher Scientific) at 1:2000 dilution for 15 min at room temperature (RT). All subsequent steps were performed in the dark. Next, cells were washed once with PBS and incubated for 15 min with BD Cytofix (BD Biosciences) at RT. After fixing, cells were washed in PBS (+3% BSA) three times and incubated in perm/wash buffer (Biolegend) for 30 min at RT. Following this incubation, cells were washed in perm/wash and incubated with conjugated antibodies: PE-Vimentin (562 337, BD Biosciences) and Alexa Fluor-647 cTnT (565 744, BD Biosciences) for 30 min at 1:10 dilution in perm/wash at RT. Cells were next washed in perm/wash and then in cell staining buffer (Biolegend) and finally resuspended in PBS. Lastly, cell events are collected in a LSRII flow

cytometer analyzer (BD Bioscience). Analysis was performed using FCS Express (De Novo Software).

Quantifying Tissue and Cellular Alignment: To quantify the alignment of aOBBs with the bioinks during printing, we must be able to identify, select, and measure their orientation. To identify individual aOBBs, all tissues were pre-incubated in three distinct fluorescent dyes with no or minimal overlapping emission spectra (CellTracker Green CMFDA (14.34×10^{-6} м), CellTracker Orange CMRA (12.1×10^{-6} м), CellTracker Deep Red (7.16×10^{-6} м)). Fluorescent dyes were diluted in DMEM High Glucose (Corning) supplemented with 50×10^{-6} м Y-27632 and incubated for 1 h at 37 °C/5.5% CO_2. After incubation, 3D images were acquired on a confocal microscope (ZEISS). The distribution of primary orientations angles (where 0° defines the direction of the print path) measured for each aOBB within the printed tissues were represented by radial histograms. To quantify cellular alignment, high magnification images (tiled scans) acquired from the center of macrofilaments were analyzed using the ImageJ plugin Directionality. The exported data from this analysis was further analyzed using CircStat, a circular statistics toolbox in Matlab, to extract resultant vector lengths; a quantifiable metric of alignment that ranges between 0 and 1.

Calcium Imaging: A 5×10^{-6} м Fluo-4 (Thermo Fischer Scientific) solution was prepared in Tyrode's solution (Alfa Aesar). The solution was supplemented to include a final concentration of 1×10^{-6} м Blebbistatin (Sigma-Aldrich) and 1×10^{-3} м Probenecid (Thermo Fischer Scientific). Bioprinted cardiac tissues were incubated with the calcium indicator for 30 min at 37 °C. Finally, the tissues were rinsed 2× in Tyrode's supplemented with Blebbistatin. The samples were illuminated by a 488 nm light. Data was acquired using Micro-Manager open-source software at 100 frames per second.

Electrical Stimulation: Bioprinted cardiac tissues were electrically stimulated using platinum wires set 8 mm apart, inserted on either side of macrofilament. A mono-phase signal with a pulse of 2 ms was generated by custom-made Arduino-based controller at a frequency of 1–3 Hz and an amplitude of 10 V cm^{-1}.

Gene Sequencing: Gene sequencing was conducted by using nanoString Elements gene sequencing platform. Prior to sequencing, bioprinted tissues were lysed in RLT buffer and RNA was extracted via Qiagen RNeasy Kit.

Statistical Analysis: Data was presented as mean ± SD unless stated otherwise. For all analyses unless explicitly stated, *t*-test or multiple *t*-tests with Holm–Sidak correction was used. In all cases, significance was defined as $p \leq 0.05$. Statistical analysis was carried out using GraphPad Prism.

Supporting Information

Supporting Information is available from the Wiley Online Library or from the author.

Acknowledgements

The authors thank W. Fabyan for his contribution to pillar array fabrication, R. Weeks for macrofilament printing assistance, D. Mau for assistance in cell culture, S. Cotreau and the Harvard SEAS Machine Shop for the manufacturing of printing platforms, and T. Ferrante for his assistance with microscopy. They are grateful to S. Das and the C. Chen lab (Boston U.) for their helpful discussions. Funding Sources: This research was primarily supported by NSF CELL-MET (#EEC-1647837) and the Vannevar Bush Faculty Fellowship Program sponsored by the Basic Research Office of the Assistant Secretary of Defense for Research and Engineering through the Office of Naval Research Grants N00014-16-1-2823 and N00014-21-1-2958. J.H.A. was supported by the NIH Ruth L. Kirschstein Predoctoral Individual National Research Service Award (#F31HL144043).

Conflict of Interest

J.A.L., J.H.A., S.G.M.U., and M.A.S.-S. have filed a patent on this work.

Author Contributions

J.H.A., S.U., M.S.-S., A.L., and J.A.L. designed research, J.H.A., S.U., M.M.M., and K.K. performed research. J.H.A., M.M.M., and J.A.L. wrote the manuscript.

Data Availability Statement

The data that support the findings of this study are available from the corresponding author upon reasonable request.

Keywords

anisotropic organ building blocks, bioprinting, cardiomyocytes, engineered cardiac tissue

Received: January 9, 2022
Revised: April 5, 2022
Published online:

[1] C. C. Beladan, A. Călin, M. Roşca, C. Ginghină, B. A. Popescu, *Heart* **2014**, *100*, 731.
[2] F. Triposkiadis, G. Giamouzis, K. D. Boudoulas, G. Karagiannis, J. Skoularigis, H. Boudoulas, J. Parissis, *Eur. J. Heart Failure* **2018**, *20*, 436.
[3] D. E. Sosnovik, A. Tawakol, *JACC: Cardiovasc. Imaging* **2018**, *11*, 1257.
[4] D. E. Sosnovik, C. Mekkaoui, S. Huang, H. H. Chen, G. Dai, C. T. Stoeck, S. Ngoy, J. Guan, R. Wang, W. J. Kostis, M. P. Jackowski, V. J. Wedeen, S. Kozerke, R. Liao, *Circulation* **2014**, *129*, 1731.
[5] D. E. Sosnovik, R. Wang, G. Dai, T. Wang, E. Aikawa, M. Novikov, A. Rosenzweig, R. J. Gilbert, V. J. Wedeen, *Circ.: Cardiovasc. Imaging* **2009**, *2*, 206.
[6] P. Garcia-Canadilla, H. Dejea, A. Bonnin, V. Balicevic, S. Loncaric, C. Zhang, C. Butakoff, J. Aguado-Sierra, M. Vázquez, L. H. Jackson, D. J. Stuckey, C. Rau, M. Stampanoni, B. Bijnens, A. C. Cook, *Circ.: Cardiovasc. Imaging* **2018**, 11.
[7] F. Weinberger, I. Mannhardt, T. Eschenhagen, *Circ. Res.* **2017**, *120*, 1487.
[8] B. M. Ogle, N. Bursac, I. Domian, N. F. Huang, P. Menasché, C. E. Murry, B. Pruitt, M. Radisic, J. C. Wu, S. M. Wu, J. Zhang, W.-H. Zimmermann, G. Vunjak-Novakovic, *Sci. Transl. Med.* **2016**, *8*, 342ps13.
[9] E. Tzatzalos, O. J. Abilez, P. Shukla, J. C. Wu, *Adv. Drug Delivery Rev.* **2016**, *96*, 234.
[10] J. Zhang, W. Zhu, M. Radisic, G. Vunjak-Novakovic, *Circ. Res.* **2018**, *123*, 244.
[11] P. Bose, J. Eyckmans, T. D. Nguyen, C. S. Chen, D. H. Reich, *ACS Biomater. Sci. Eng.* **2019**, *5*, 3843.
[12] N. Bursac, K. K. Parker, S. Iravanian, L. Tung, *Circ. Res.* **2002**, *91*, e45.
[13] A. S. T. Smith, H. Yoo, H. Yi, E. H. Ahn, J. H. Lee, G. Shao, E. Nagornyak, M. A. Laflamme, C. E. Murry, D.-H.o Kim, *Chem. Commun.* **2017**, *53*, 7412.
[14] Y. Wu, L. Wang, B. Guo, P. X. Ma, *ACS Nano* **2017**, *11*, 5646.
[15] R. J. Wade, E. J. Bassin, C. B. Rodell, J. A. Burdick, *Nat. Commun.* **2015**, *6*, 6639.

[16] L. A. Macqueen, S. P. Sheehy, C. O. Chantre, J. F. Zimmerman, F. S. Pasqualini, X. Liu, J. A. Goss, P. H. Campbell, G. M. Gonzalez, S.-J. Park, A. K. Capulli, J. P. Ferrier, T. F. Kosar, L. Mahadevan, W. T. Pu, K. K. Parker, *Nat. Biomed. Eng.* **2018**, *2*, 930.
[17] J. Schwan, A. T. Kwaczala, T. J. Ryan, O. Bartulos, Y. Ren, L. R. Sewanan, A. H. Morris, D. L. Jacoby, Y. Qyang, S. G. Campbell, *Sci. Rep.* **2016**, *6*, 32068.
[18] W. R. Legant, A. Pathak, M. T. Yang, V. S. Deshpande, R. M. Mcmeeking, C. S. Chen, *Proc. Natl. Acad. Sci. USA* **2009**, *106*, 10097.
[19] H. Vandenburgh, J. Shansky, F. Benesch-Lee, V. Barbata, J. Reid, L. Thorrez, R. Valentini, G. Crawford, *Muscle Nerve* **2008**, *37*, 438.
[20] A. Grosberg, P. W. Alford, M. L. Mccain, K. K. Parker, *Lab Chip* **2011**, *11*, 4165.
[21] W.-H. Zimmermann, K. Schneiderbanger, P. Schubert, M. Didié, F. MüNzel, J. F. Heubach, S. Kostin, W. L. Neuhuber, T. Eschenhagen, *Circ. Res.* **2002**, *90*, 223.
[22] W. Bian, C. P. Jackman, N. Bursac, *Biofabrication* **2014**, *6*, 024109.
[23] I. Y. Shadrin, B. W. Allen, Y. Qian, C. P. Jackman, A. L. Carlson, M. E. Juhas, N. Bursac, *Nat. Commun.* **2017**, *8*, 1825.
[24] F. Weinberger, K. Breckwoldt, S. Pecha, A. Kelly, B. Geertz, J. Starbatty, T. Yorgan, K.-H. Cheng, K. Lessmann, T. Stolen, M. Scherrer-Crosbie, G. Smith, H. Reichenspurner, A. Hansen, T. Eschenhagen, *Sci. Transl. Med.* **2016**, *8*, 363ra148.
[25] A. S. Gladman, E. A. Matsumoto, R. G. Nuzzo, L. Mahadevan, J. A. Lewis, *Nat. Mater.* **2016**, *15*, 413.
[26] B. G. Compton, J. A. Lewis, *Adv. Mater.* **2014**, *26*, 5930.
[27] A. Kotikian, R. L. Truby, J. W. Boley, T. J. White, J. A. Lewis, *Adv. Mater.* **2018**, *30*, 1706164.
[28] C. Mahajan, D. Cormier, *IISE Annu. Conf. Proc.*, Institute of Industrial and Systems Engineers (IISE), Norcross, GA, USA **2015**, 2953.
[29] M. L. Shofner, K. Lozano, F. J. Rodríguez-Macías, E. V. Barrera, *J. Appl. Polym. Sci.* **2003**, *89*, 3081.
[30] C. C. Spackman, C. R. Frank, K. C. Picha, J. Samuel, *J. Manuf. Processes* **2016**, *23*, 296.
[31] M. E. Prendergast, M. D. Davidson, J. A. Burdick, *Biofabrication* **2021**, *13*, 044108.
[32] B. A. Nerger, P.-T. Brun, C. M. Nelson, *Soft Matter* **2019**, *15*, 5728.
[33] H. Kim, J. Jang, J. Park, K.-P. Lee, S. Lee, D.-M. Lee, K.i H. Kim, H. K. Kim, D.-W. Cho, *Biofabrication* **2019**, *11*, 035017.
[34] A. Schwab, C. Hélary, R. G. Richards, M. Alini, D. Eglin, M. D'este, *Mater. Today Bio* **2020**, *7*, 100058.
[35] M. Farkash, D. G. Brandon, *Mater. Sci. Eng., A* **1994**, *177*, 269.
[36] K. D. Costa, E. J. Lee, J. W. Holmes, *Tissue Eng.* **2003**, *9*, 567.
[37] E. J. Lee, J. W. Holmes, K. D. Costa, *Ann. Biomed. Eng.* **2008**, *36*, 1322.
[38] D. Mukhija, M. J. Solomon, *Soft Matter* **2011**, *7*, 540.
[39] M.-T. Zhao, S. Ye, J. Su, V. Garg, *Front. Cell Dev. Biol.* **2020**, *8*, 594226.
[40] N. Huebsch, P. Loskill, N. Deveshwar, C. I. Spencer, L. M. Judge, M. A. Mandegar, C. B. Fox, T. M. A. Mohamed, Z. Ma, A. Mathur, A. M. Sheehan, A. Truong, M. Saxton, J. Yoo, D. Srivastava, T. A. Desai, P.o-L. So, K. E. Healy, B. R. Conklin, *Sci. Rep.* **2016**, *6*, 24726.
[41] M. A. Skylar-Scott, S. G. M. Uzel, L. L. Nam, J. H. Ahrens, R. L. Truby, S. Damaraju, J. A. Lewis, *Sci. Adv.* **2019**, *5*, eaaw2459.
[42] X. Lian, J. Zhang, S. M. Azarin, K. Zhu, L. B. Hazeltine, X. Bao, C. Hsiao, T. J. Kamp, S. P. Palecek, *Nat. Protoc.* **2012**, *8*, 162.